ACCOUNTS of chemical research

pubs.acs.org/accounts Article

Exploring Anomalous Fluid Behavior at the Nanoscale: Direct Visualization and Quantification via Nanofluidic Devices

Junjie Zhong,[⊥] Mohammad Amin Alibakhshi,[⊥] Quan Xie,[⊥] Jason Riordon, Yi Xu, Chuanhua Duan,* and David Sinton*

Cite This: https://dx.doi.org/10.1021/acs.accounts.9b00411 Read Online

ACCESS | Metrics & More | Article Recommendations

CONSPECTUS: Nanofluidics is the study of fluids under nanoscale confinement, where small-scale effects dictate fluid physics and continuum assumptions are no longer fully valid. At this scale, because of large surface-area-to-volume ratios, the fluid interaction with boundaries becomes more pronounced, and both short-range steric/hydration forces and long-range van der Waals forces and electrostatic forces dictate fluid behavior. These forces lead to a spectrum of anomalous transport and thermodynamic phenomena such as ultrafast water flow, enhanced ion transport, extreme phase transition temperatures, and slow biomolecule diffusion, which have been the subject of extensive computational studies. Experimental quantification of these phenomena was also enabled by the advent of nanofluidic technology, which has transformed challenging nanoscale fluid measurements into facile optical and electrical recordings.

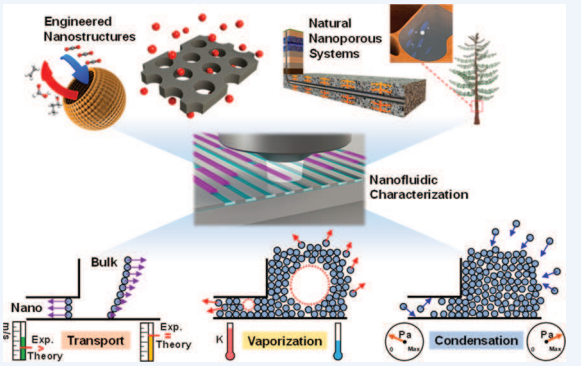

Our groups' focus is to investigate nanoscale (2 to 10^3 nm) fluid behaviors in the context of fluid mechanics and thermodynamics through the development of novel nanofluidic tools, to examine the applicability of classical equations at the nanoscale, to identify the source of deviations, and to explore new physics emerging at this scale. In this Account, we summarize our recent findings regarding liquid transport, vaporization, and condensation of nanoscale-confined liquids.

Our study of nanoscale water transport identified an additional resistance in hydrophilic nanochannels, attributed to the reduced cross-sectional area caused by the formation of an immobile hydration layer on the surfaces. In contrast, a reduction in flow resistance was discovered in graphene-coated hydrophobic nanochannels, due to water slippage on the graphene surface. In the context of vaporization, the kinetic-limited evaporation flux was measured and found to exceed the classical theoretical prediction by an order of magnitude in hydrophilic nanochannels/nanopores as a result of the thin film evaporation outside of the apertures. This factor was eliminated by modifying the hydrophobicity of the aperture's exterior surface, enabling the identification of the true kinetic limits inside nanoconfinements and a crucial confinement-dependent evaporation coefficient. The transport-limited evaporation dynamics was also quantified, where experimental results confirmed the parallel diffusion−convection resistance model in both single nanoconduits and nanoporous systems at high accuracy. Furthermore, we have extended our studies to different aspects of condensation in nanoscale-confined spaces. The initiation of condensation for a single-component hydrocarbon was observed to follow the Kelvin equation, whereas for hydrocarbon mixtures it deviated from classical theory because of surface-selective adsorption, which has been corroborated by simulations. Moreover, the condensation dynamics deviates from the bulk and is governed by either vapor transport or liquid transport depending on the confinement scale. Overall, by using novel nanofluidic devices and measurement strategies, our work explores and further verifies the applicability of classical fluid mechanics and thermodynamic equations such as the Navier−Stokes, Kelvin, and Hertz−Knudsen equations at the nanoscale. The results not only deepen our understanding of the fundamental physical phenomena of nanoscale fluids but also have important implications for various industrial applications such as water desalination, oil extraction/recovery, and thermal management. Looking forward, we see tremendous opportunities for nanofluidic devices in probing and quantifying nanoscale fluid thermophysical properties and more broadly enabling nanoscale chemistry and materials science.

1. INTRODUCTION

Nanofluidic systems, in which fluid is confined at the scales from single atoms all the way to the Debye screening length and beyond, are powerful tools for investigating nanoscale fluid mechanics, thermodynamics, electrokinetics,[1] and biophysics.[2]

Received: July 31, 2019

The experimental study of nanoscale fluid behavior is uniquely important, as it not only provides theoretical understanding but also offers guidelines to advance engineering frontiers in the clean energy,[3] lab-on-a-chip,[4] chemical analysis,[5] and oil/gas industries.[6] Conducting such experiments, however, is notoriously challenging because of the difficulties inherent to creating a relevant nanoconfined system and collecting data from the ultrasmall volumes within. The experimental study of nanoscale fluids conducted with nanoporous media[7] provides valuable insights into the complexity of such systems, where nanoscale fluid behaviors are measured by averaging over the entire nanoporous medium, with internal variations in pore sizes and surfaces. However, nanoscale fluid behaviors are intensely geometry-dependent and localized, and classical medium-averaged experimental methods cannot fully resolve these behaviors. One way to resolve this issue is to study nanoscale fluid behaviors using individual nanoconduits with well-defined geometries and better-controlled surfaces compared with nanoporous media. Recent progress in nanofluidic device fabrication and measurement techniques has opened a window for direct visualization of fluid phases at the nanoscale (which is not possible with nanoporous media) and enabled real-time quantification of fluid behaviors down to the scale of a few nanometers.[8]

Among all existing nanofluidic devices, the planar nanochannel device has been the most widely used. While the nanochannel height creates one-dimensional confinement, the nanochannel width is relatively large (in the range of 2−50 μm, or ∼100−1000 times the channel height) to enable direct observation by optical microscopy. Nevertheless, the complex nature of nanoscale fluid studies entails further incorporation of creative designs and novel microfabrication schemes to facilitate characterization and measurement of nanofluidic systems. Beyond planar nanochannels, we have focused for the last 5 years on the smart design of fluidic systems and the development of a nanofluidic toolbox for probing mass transport and thermodynamic processes under precisely controlled conditions (i.e., temperature, pressure, and relative humidity). Some of the novel features incorporated into our designs include the integration of different forms of nanoconfinement (e.g., nanochannels and nanopores), graphene coating, optical enhancement layers, and two-dimensional (2D) replicas of nanoporous media, focusing on confinements in the range of 2 to 10^3 nm.

We have applied this new generation of devices to detect and characterize important confinement-dependent fluid behaviors, including reduced/enhanced liquid flow, reduced mixture bubble points/dew points, and ultrahigh kinetic-limited evaporation fluxes (Figure 1). These studies are grouped into three major topics in this Account: (i) liquid transport, (ii) evaporation and bubble nucleation, and (iii) condensation. Each section summarizes our novel experimental approach and key findings. We conclude with a discussion on the role of nanofluidic devices in promoting nanoscale fluid behavior studies and provide an outlook on potential challenges and opportunities for future nanofluidic devices and studies.

2. FLUID TRANSPORT AT THE NANOSCALE

The validity of classical fluid dynamics at the nanoscale has been challenged since the first direct observation of water entering hydrophobic nanoscale conduits.[9] It has recently been observed that water flow at the nanoscale is strongly associated

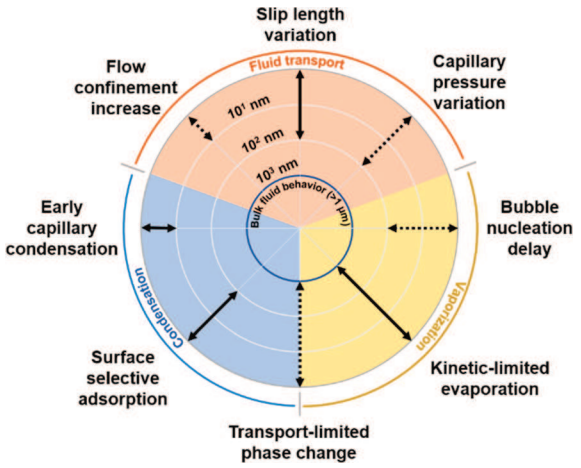

Figure 1. Key anomalies of nanoscale fluid behaviors. The double-sided arrows indicate the dimensions of interest for different anomalies and whether they promote (solid) or impede (dashed) fluid behaviors compared with classical bulk fluid theories.

with surface properties and that the flow rates can be greatly enhanced in atomically smooth, hydrophobic nanoconduits.[10,11] These anomalous transport phenomena suggest that classical fluid dynamics and bulk liquid properties (viscosity, density, interfacial tension, etc.) cannot fully describe nanoscale fluid dynamics and that further investigation is required for a better understanding of the fundamental mechanisms.

However, just as classical theories are not necessarily applicable at the nanoscale, it is very challenging to use classical experimental methodologies to accurately quantify fluid transport under nanoconfinements because of the enormous flow resistance, the ultralow flow rate, and the ultrahigh pressure gradient. Thankfully, capillary flow inside planar nanochannels is favored and provides sufficient pressure to overcome these challenges. Planar nanoslits also allow for the capillary flow rate to be accurately measured by tracking the meniscus advancing length as a function of time, which is expected to follow the Lucas−Washburn equation.[12,13] However, in this equation, the nanochannel flow resistance and the capillary pressure are coupled in one term, and the capillary pressure is estimated on the basis of the classical Young−Laplace equation and bulk liquid properties, including surface tension and macroscale contact angles. Relying on such a theoretical pressure estimation overlooks a range of nanoscale fluid phenomena and inhibits a clear understanding of flow characteristics at this scale. We developed a novel hybrid nanochannel scheme to measure the nanochannel flow resistance without estimating the capillary pressure (Figure 2a,b).[14] Briefly, the nanochannel with unknown resistance is seamlessly connected to a reference channel with known flow resistance. Capillary filling along such a hybrid nanochannel would follow a modified Lucas−Washburn equation containing an additional term that is related only to the mass-flow resistance ratio between the test and reference nanochannels. Conducting two capillary filling experiments from the test and reference channel ends and establishing two Lucas−Washburn equations allows the capillary pressure term to be internally canceled from these two equations, and the flow resistance of the test channel can be calculated unambiguously.

Using this technique, we studied water transport in hydrophilic silica nanochannels (Figure 2c). Compared with

https://dx.doi.org/10.1021/acs.accounts.9b00411
Acc. Chem. Res. XXXX, XXX, XXX−XXX

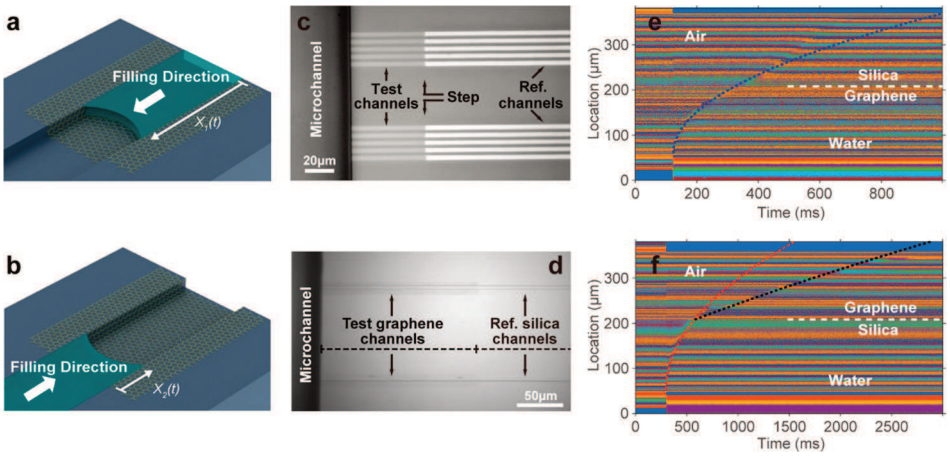

Figure 2. Hybrid nanochannel scheme for the nanoscale flow resistance measurement. Two capillary filling experiments starting from (a) a test channel (covered by graphene) and (b) a reference channel (without graphene coverage) can decouple the capillary pressure and the flow resistance. (c) Hybrid channel for sub-10 nm silica nanochannel flow resistance measurements. (d) Hybrid channel for graphene nanochannel flow resistance measurements. (e, f) Meniscus location as a function of time for the capillary filling experiments starting from the (e) left and (f) right ends of the hybrid graphene nanochannel shown in (d). The choice of the colormap is essential for visualization and enhancement of the water/air contrast. (a, b, d–f) Reproduced with permission from ref 15. Copyright 2018 Nature Publishing Group. (c) From ref 14. CC BY 4.0.

classical theories with a no-slip boundary condition, a 45% increase in water flow resistance in 7 nm nanochannels was observed (Figure 3a), and the deviation of the water flow resistance decreased as the height of the nanochannel increased.[14] We attributed this flow resistance increase to the strong interaction between water molecules and the hydrophilic surfaces. For silica surfaces, two or three layers of water molecules tend to reorient themselves into ordering layers, resulting in an ice-like hydration layer near the substrate. This hydration layer reduces the effective nanochannel height and leads to an increase in flow resistance.

We also studied water transport in graphene nanochannels (prepared by coating silica nanochannels with graphene on the bottom and side walls, 24–124 nm in height) with the same technique (Figure 2d–f).[15] Our results showed that the water flow resistance of three-side-covered graphene nanochannels, despite an unexpectedly large variation, can be up to 4 times smaller than the flow resistance of silica nanochannels with the same dimensions, which suggests interfacial slip between water and the graphene surface (Figure 3c). We calculated the slip length (see Figure 3b for definition) of graphene based on the measured flow resistance and found that there is a wide distribution of slip lengths (1–200 nm), which can be attributed to varied surface charge density on the graphene surface. We also found that the statistical median of the slip length (~16 nm) aligns very well with the reported value for large-diameter carbon nanotubes (~17 nm).[10]

As this technique can decouple the capillary pressure and flow resistance, we also used this method to measure the capillary pressure in graphene nanochannels and correlated it with the flow resistance as well as the graphene coverage and quality (Figure 3d,e). Our results indicate that the capillary pressure in three-side-covered graphene nanochannels is significantly lower than predictions based on the classical Young–Laplace equation (assuming a contact angle of 0°) because of the large contact angle of the graphene surface. While higher graphene coverage in the graphene nanochannel leads to lower capillary pressure and low flow resistance, low graphene coverage not only increases the magnitude of the capillary pressure but also results in increased flow resistance compared with silica nanochannels, possibly because of additional interfacial flow resistance between hydrophilic and hydrophobic regions (Figure 3c–e).

Overall, our unambiguous measurements of water transport in individual silica and graphene nanochannels provide experimental support for recent theoretical studies on the effect of wettability on nanoscale water transport.[16,17] Consequently, it is possible to predict water transport in nanoconfinements (2 to 10^3 nm) using the classical hydrodynamics equation along with wettability-dependent viscosity and slip length[16] provided that the water contact angle (wettability) can be accurately measured/estimated in the system. However, for ultrasmall nanoconfinements (sub-2 nm), further experimental investigation is needed because the limits of the continuum assumption are reached.

The measured graphene slip length and its dependence on the surface charge density offer design guidelines for new graphitic membranes and nanofluidic devices relevant to emerging applications in nanofiltration and energy haverst-ing.[18] In particular, it is possible to develop novel graphene/graphene oxide laminate membranes with high selectivity and high permeation capacity for water desalination by forward osmosis, which can be operated at a much lower energy cost than reverse osmosis.[18]

3. VAPORIZATION AT THE NANOSCALE

Vaporization of nanoscale-confined liquids is ubiquitous in nature and plays a critical role in many important applications, including energy conversion,[19] solar steam generation,[20] and electronics cooling. We have investigated the thermodynamics of vaporization in nanoconfined spaces, including kinetic-limited evaporation at the liquid–vapor interface, vaporization of nanoscale-confined liquids, and nanoscale bubble nucleation and growth. The following subsections present a synopsis and highlights of our recent studies in this area.

3.1. Kinetic-Limited Evaporation from Nanoscale Apertures

The maximum evaporation flux in any system is determined by the evaporation kinetics at the liquid–vapor interface. However, the so-called kinetic-limited evaporation flux,

https://dx.doi.org/10.1021/acs.accounts.9b00411
Acc. Chem. Res. XXXX, XXX, XXX–XXX

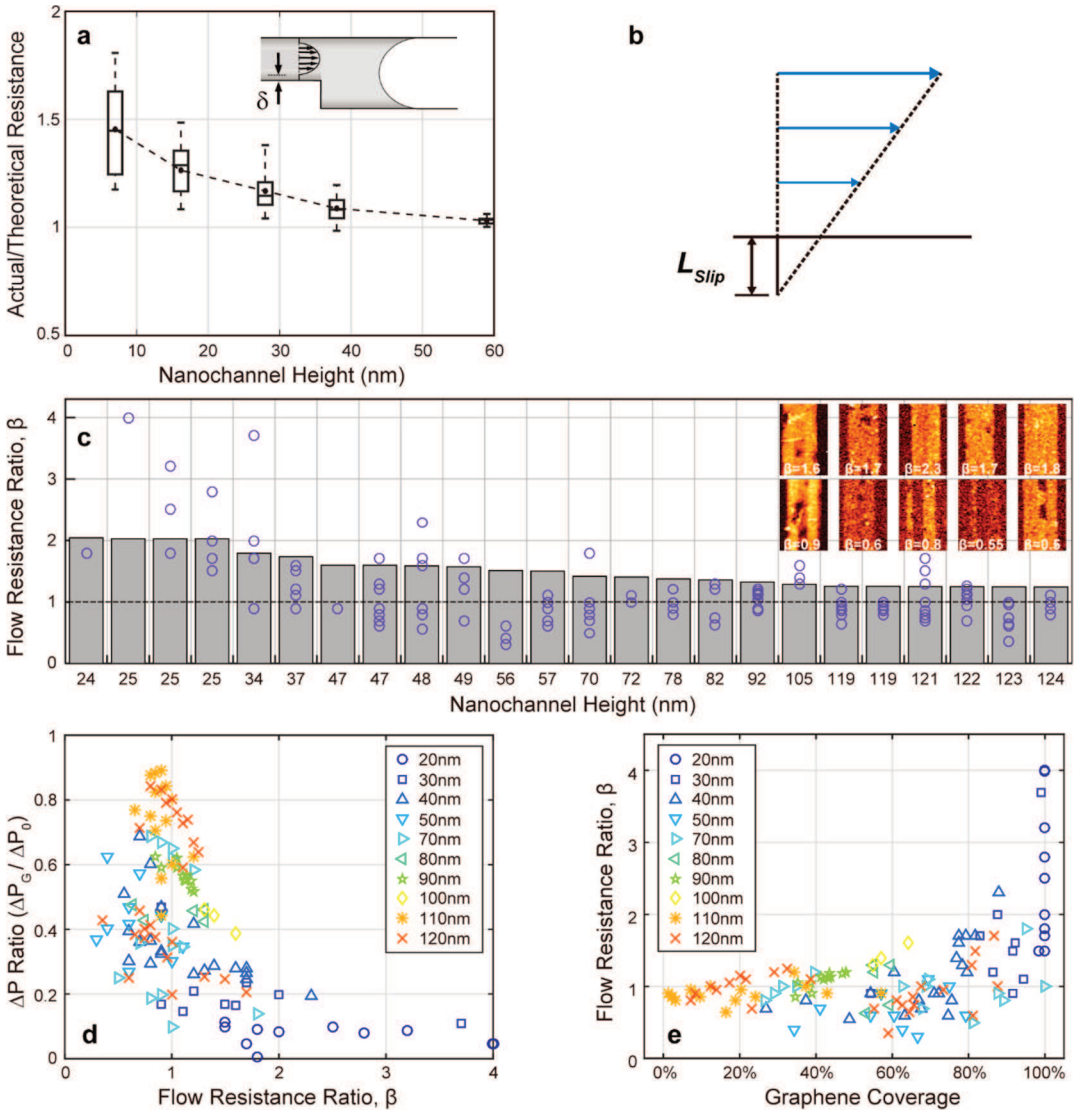

Figure 3. Flow resistance and capillary pressure in nanochannels. (a) Flow resistance of a silica nanochannel vs the nanochannel height. (b) Schematic of the slip length. (c) Flow resistance ratio between the silica and graphene nanochannels (β) vs the nanochannel height. Gray bars represent theoretical calculations assuming a constant slip length of 10 nm, and blue circles represent experimental results. Inset: graphene coverage inside channels labeled with the corresponding β values. (d) Correlation between the capillary pressure and the flow resistance in graphene nanochannels. (e) Correlation between the flow resistance and the graphene coverage in graphene nanochannels. (a) From ref 14. CC BY 4.0. (c–e) Reproduced with permission from ref 15. Copyright 2018 Nature Publishing Group.

which is generally believed to be described by the Hertz–Knudsen equation,[21] is impossible to achieve at the macro/microscale liquid–vapor interface, as heat/mass transfer to the interface becomes the dominant limiting factor. In contrast, confinement of liquids at the nanoscale could facilitate heat/liquid transfer to the interface because of minimized liquid thermal resistance and prominent capillary action, which thus may enable evaporation to reach the kinetic limit. However, at the nanoscale, more sophisticated physics, including confinement-induced changes in water structures and evaporation area, as well as evaporation and recondensation at highly curved interfaces may also affect phase change at the interface. These challenges therefore require more comprehensive modeling of the nanoscale liquid–gas interface and the development of experimental methods for accurate measurement of infinitesimal evaporation fluxes. Here we provide an overview of our recent achievements in exploring kinetic-limited evaporation from circular/rectangular nanoscale apertures.

The challenge in characterizing evaporation from nanoscale apertures, i.e., 1D slit (height ≪ width) or 2D circular apertures, arises from the small amount of mass under study. We tackled this challenge by integrating a to-be-tested nanoscale aperture with a long reference channel and converting evaporation rate/flux measurements into tracking of a receding meniscus in the nanochannel during a drying process (Figure 4a–d). Our experimental results for hydrophilic silica rectangular apertures showed that the kinetic-limited evaporation flux increases monotonically as the aperture height decreases (Figure 4e). At the elevated temperature of 40 °C, a very large evaporation flux of 37.5 mm/s was recorded from a 16 nm-high rectangular aperture; this value is ∼5 times the Hertz–Knudsen prediction (assuming an evaporation coefficient equal to 1) and corresponds to a heat flux of 8500 W/cm^2.[22] Such high

https://dx.doi.org/10.1021/acs.accounts.9b00411
Acc. Chem. Res. XXXX, XXX, XXX–XXX

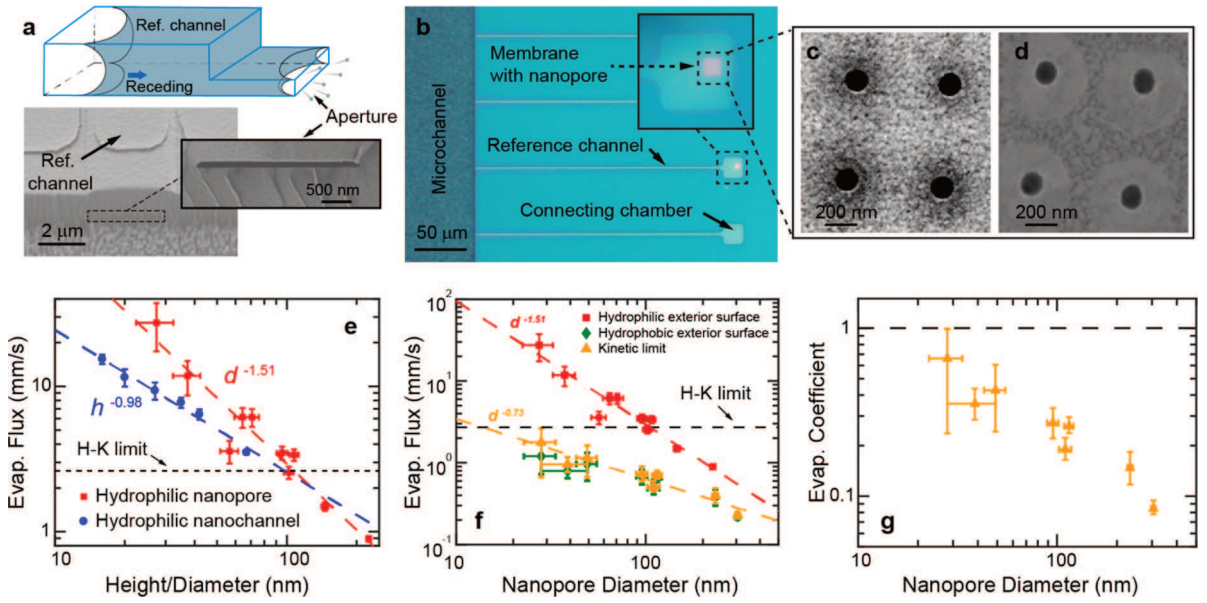

Figure 4. Kinetic-limited evaporation from 1D and 2D nanoscale apertures. (a) Scanning electron microscopy image of a hybrid nanochannel with a rectangular aperture. (b) Microscope image of a nanochannel-integrated nanopore device. (c, d) Nanopores with (c) hydrophilic and (d) hydrophobic exterior surfaces were used for the experiments. (e) Dependence of the evaporation flux on 1D and 2D confinements in hydrophilic nanochannels and nanopores. (f) Evaporation fluxes from nanopores with hydrophobic and hydrophilic exterior surfaces. (g) Evaporation coefficient as a function of nanopore diameter. Reproduced from (a) ref 22 and (b–g) ref 23. Copyright 2017 and 2019, respectively, American Chemical Society.

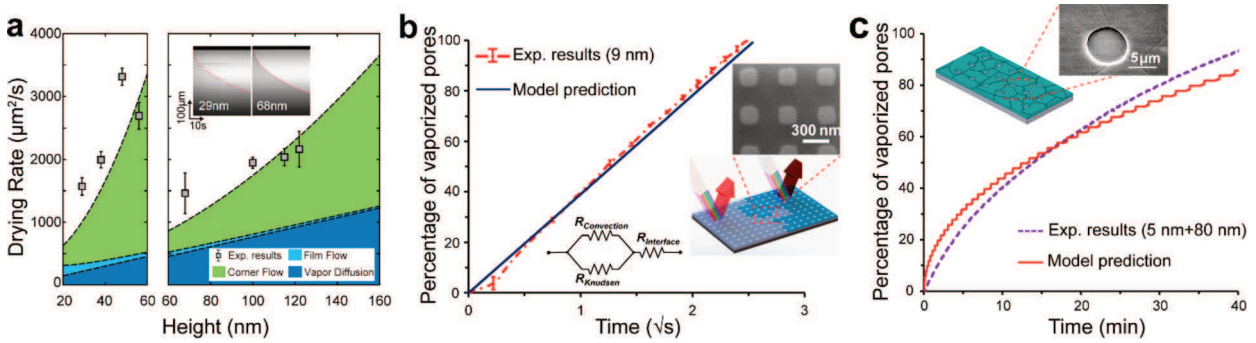

Figure 5. Evaporation of nanoscale-confined liquids. (a) Experimental water drying rates in individual nanochannels of different heights and contributions of different mechanisms to the drying rate. (b, c) Experimental results and dynamic model predictions of (b) propane evaporation dynamics in a 9 nm nanogrid and (c) capillary evaporation of a methane/propane/pentane (1:4:5) mixture in a 5 nm nanogrid connecting 80 nm-deep nanopore arrays. Reproduced (a) from ref 25, (b) from ref 27, and (c) with permission from ref 28. Copyright 2017 and 2018 American Chemical Society and 2019 Royal Society of Chemistry, respectively.

kinetic-limited evaporation fluxes were later found mainly to result from an evaporating thin film outside of the nanochannel.[11] When we used the same technique to measure kinetic-limited water evaporation from 2D circular nanopores, which are a more realistic model of many natural and industrial systems, we found similar trends and even higher evaporation fluxes.[23] Our results from hydrophilic silicon nitride nanopores show that the evaporation flux versus nanopore diameter (d) scales as $d^{-1.51}$, reaching 11 times the Hertz–Knudsen limit for a 27 nm nanopore (Figure 4e). However, experiments conducted using KCl solutions instead of deionized water revealed the formation of KCl crystals outside the nanopore area, indicating the presence of an evaporating thin film outside of the aperture. Modification of the nanopore exterior by a 1-octanethiol self-assembled hydrophobic layer (Figure 4d) eliminated the formation of KCl crystals, which suggests that the meniscus was pinned at the nanopore. The evaporation flux in such nanopores scales as $d^{-0.73}$ and is reduced to below the Hertz–Knudsen limit (Figure 4f). This dependence of the kinetic limit on the nanopore diameter can only be explained by a confinement-dependent evaporation coefficient (Figure 4g), possibly due to surface-charge-induced concentration changes of hydronium ions in nanopores.[23]

Our findings suggest that by considering a confinement-dependent evaporation coefficient, one can still use the classical kinetic theory to predict kinetic-limited evaporation performance, which was also verified by a recent experimental study based on ultrathin nanoporous membranes.[24] These findings may further inspire the development of new nanoporous evaporators for membrane distillation, solar-driven interfacial evaporation, and thermal management. Specifically, ultrathin nanoporous membrane evaporators with small nanopores and high porosities may achieve unprecedented

https://dx.doi.org/10.1021/acs.accounts.9b00411
Acc. Chem. Res. XXXX, XXX, XXX–XXX

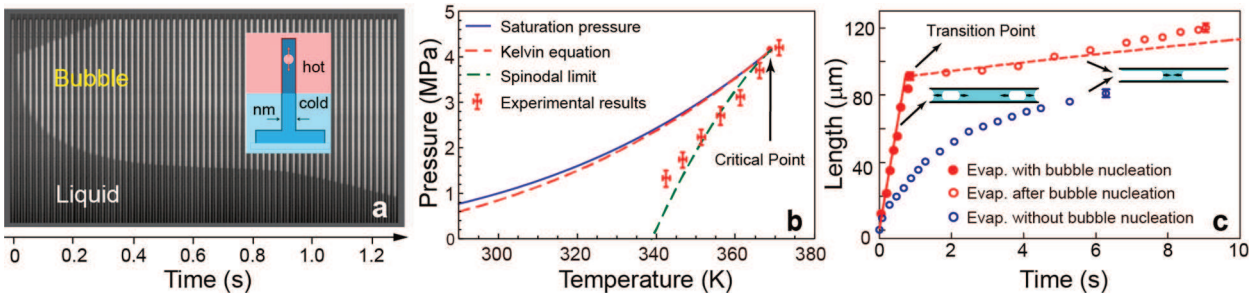

Figure 6. (a) Schematic and observation of pressure/temperature-change-induced bubble nucleation and growth of propane in an 88 nm-deep channel, with the initiation condition shown in (b) compared with theoretical predictions. The experimental results are close to the liquid spinodal limit. (c) Water evaporation with or without bubble nucleation in a 20 nm channel. The bubble growth rate difference between the two cases is up to 35 times. (a, b) Reproduced with permission from ref 32. Copyright 2017 The PCCP Owner Societies. (c) Reproduced from ref 31. Published by the National Academy of Sciences.

heat dissipation rates, providing new approaches to cool high-power electronics.

3.2. Evaporation of Nanoscale-Confined Liquids

When the vaporization interface is confined within the nanoconduit, both the liquid and vapor phases across the interface are confined at the same nanoscale (in contrast, at the nanoconduit entrance, the vapor phase is not confined at the nanoscale), and liquid/vapor removal is no longer efficient. The evaporation flux is commonly determined by the liquid/vapor transport in the nanoconduit toward/from the interface. We used 1D planar nanochannels as model systems to explore this evaporation regime (Figure 5a).[25] Our results show that the effective water vapor diffusivity inside hydrophilic nanochannels (29−122 nm deep) is close to that predicted by Knudsen theory because of the joint effects of strong water adsorption on hydrophilic surfaces and the specular collision of vapor molecules. In addition, we observed that corners of hydrophilic nanochannels can hold water and enhance the liquid removal rate during the drying process. The contribution of corner flows[26] is dependent only on the geometry of the channels and can be significant if the corner is sharp (Figure 5a).

We also measured the hydrocarbon evaporation flux in nanogrids, i.e., fully connected networks of 2D nanochannels (Figure 5b) that mimic nanoporous media in both natural (biological, geological) and synthetic (membrane) systems. In contrast to nanoslits, nanogrids guarantee negligible liquid corner flow effects. Thus, the evaporation flux is mainly governed by the vapor transport resistance, including convection and diffusion. We found that this resistance can be 5 orders of magnitude greater than the kinetic-limited interfacial resistance at a sub-10 nm scale.[27] Clear visualization of fluid phases at the sub-10 nm scale was challenging in previous nanofluidic devices and was achieved here by adding an optical contrast enhancement layer.[8] A theoretical model based on the vapor transport resistance was developed and showed high predictability for single-component hydrocarbons in a single-dimension nanogrid[27] (Figure 5b) and hydrocarbon mixtures in a multidimension nanogrid (Figure 5c).[28] The validated model contains no fitting parameters and can be readily applied to nanoporous systems more generally, provided that the effect of nanoconfinement impeding vapor transport is significant, vapor transport is in the transitional region, and the continuum assumption remains reasonable (Knudsen number = 0.1−1). However, in extremely small nanoconfinements (e.g., sub-2 nm), where the confinement dimension is much smaller than the gas molecule mean free path and close to the molecule size (i.e., Knudsen number >10), the model developed here is no longer applicable, and quantum effects can trigger much faster gas flow than classical theory predicts.[29]

The significantly reduced vaporization rate for liquid confined in nanoporous media indicates the inefficiency of producing heavy fractions in shale gas/oil through primary recovery (fast production decay after a few months) and motivates enhanced recovery strategies such as CO_2 injection. Our findings further indicate that geological storage of CO_2 injected into nanoporous reservoirs is possible, as CO_2 release will be inhibited as a nanoconfined gas.[30] Combining recovery with CO_2 storage could provide an economically feasible route to near-term CO_2 storage in nanoporous media.

3.3. Bubble Nucleation and Growth at the Nanoscale

Another nanoscale vaporization phenomenon is cavitation, i.e., bubble nucleation/growth in nanoscale-confined liquids. Cavitation in nanoconfinement is relevant to many biological and industrial processes yet has remained largely unexplored because of the lack of applicable methods. Quantifying bubble nucleation at the nanoscale is challenging, as it requires clear evidence of detection of nanobubbles in addition to quantification of the vapor content change. These challenges were circumvented using nanofluidic devices that allow direct fluid phase identification down to the sub-10 nm regime.

Liquid confined at the nanoscale can sustain a high tension and therefore be metastable. Cavitation at the nanoscale is generally believed to be energetically unfavorable, as the diameter required for vapor bubble nucleation is close to the smallest confinement size.[31] We directly measured bubble nucleation thermodynamic conditions in a nanochannel. An experimental system was designed to isolate bubble nucleation from evaporation through a temperature gradient integrated within the chip (Figure 6a).[32] In this case, the initiation pressure of bubble nucleation for a single-component liquid (e.g., propane) in nanoconfinement was found to be significantly lower than the pressure predicted by the bulk saturation curve, and conditions approached the liquid spinodal limit (liquid unstable limit) (Figure 6b).[32]

Following nucleation, the underlying mechanism of nanoscale-confined bubble growth is another topic of much interest (Figure 6c).[31] Although the very high negative capillary pressures imposed on confined liquid water in nanochannels generally preclude bubble nucleation[33] (water becomes metastable and approaches the spinodal limit), we found that

https://dx.doi.org/10.1021/acs.accounts.9b00411
Acc. Chem. Res. XXXX, XXX, XXX−XXX

nanochannels with tapered entrances allow air pockets to enter the nanochannels and form a bubble. Such devices were employed to study bubble growth in nanochannels. Once a bubble is introduced and trapped inside a nanochannel, it can act as a nucleus and grow, while the menisci are pinned at the nanochannel entrances. Since there is no vapor transport along the nanochannel, the overall vaporization length is proportional to time ($L \propto t$). Thus, compared with transport-limited evaporation ($L \propto \sqrt{t}$), the overall vaporization rate shows a significant increase. The vaporization rate in the presence of a bubble in a 20 nm-deep and 120 μm-long nanochannel was found to be 35-fold higher than the evaporation rate without bubble nucleation (Figure 6c).[31] These results describe a potential mechanism behind the fast drying behavior of porous materials.[34]

4. CONDENSATION AT THE NANOSCALE

Capillary condensation at the nanoscale is essential in many engineering processes, such as heat management through nanostructured surfaces,[35] water/energy harvesting with nanoporous materials,[36] and shale gas production.[6] We studied nanoscale capillary condensation from two different perspectives: (i) the thermodynamic initiation point and (ii) the condensate growth dynamics.

We performed experiments with both a single-component gas (propane) and a gas mixture (80% propane + 20% methane), exploring condensation in planar nanochannels with heights of 8 and 80 nm by directly observing the initiation of the liquid phase from the vapor (Figure 7a). We found that for the single-component nonpolar gas molecules, the Kelvin equation derived from classical thermodynamics provides accurate predictions down to the sub-10 nm regime.[37] The maximum deviation between the dew point measurements and the Kelvin equation predictions was only 8%. However, for the gas mixture, the dew point in the nanochannels deviates significantly from the Kelvin equation. We measured dew point reductions of up to 129% at 8 nm (Figure 7b).[37] This significant deviation is inherently correlated with preferential adsorption of heavier molecules on the nanochannel surface, leading to a denser liquid composition in the nanochannel compared with that in the bulk at the dew point (a density functional theory calculation showed that the propane/methane ratio is 13% higher in the 8 nm nanochannel compared with the bulk), and thus, condensation occurs at a much lower pressure than predicted by the Kelvin equation.[37] Such surface-selectivity-induced early condensation for gas mixtures is unique at the nanoscale, as surface-adsorbed components significantly affect the molecular distribution in nanopores because of the large surface-area-to-volume ratio.[38] The preferential surface adsorption enriching the heavy fluid composition in nanoconfinement presents additional applications in homogeneous catalysis. For example, in the electrochemical reduction of CO, nanocavity-shaped copper catalysts have been shown to trap intermediates and produce higher-carbon C3 products (e.g., propanol).[39]

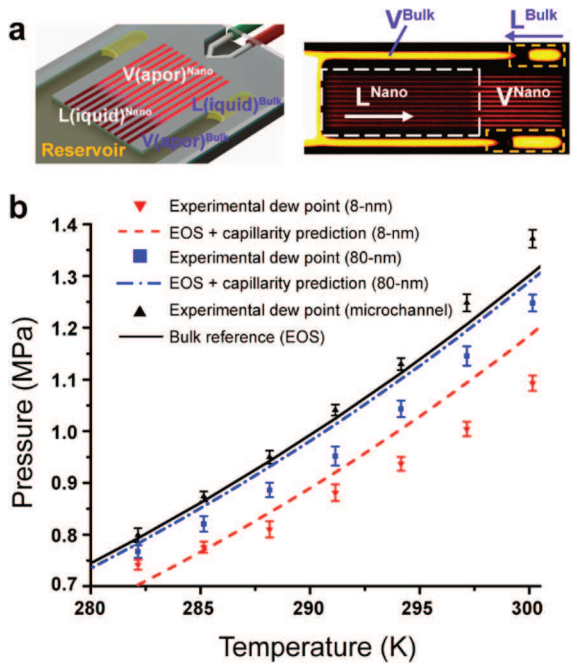

Figure 7. Initiation of capillary condensation within nanofluidic devices. (a) Schematic of the nanofluidic chip setup and results of direct observations of vapor condensation in 8 nm-deep nanochannels and the bulk (microchannel). (b) Experimental results of tested condensation initiation in 8 and 80 nm channels compared with predictions from classical equations. Reproduced from (a) ref 40 and (b) ref 37. Copyright 2018 American Chemical Society.

We also quantified the condensation dynamics in the nanoscale-confined case. For capillary condensation confined at tens of nanometers (e.g., 70 nm) and above, we found that the condensate initiates from the nanochannel dead end because of the additional wall surface and grows toward the channel entrance. In addition to the condensation kinetic resistance at the liquid−vapor interface, the vapor transport resistance in nanochannels significantly affects the condensate growth rate, contributing over 70% of the total resistance.[41] In such cases, pressure-driven gas convection and Knudsen diffusion in parallel contribute to the vapor transport (Figure 8a). By combining the three effective resistances, we proposed a theoretical model that can closely predict the experimental results (Figure 8c). When the confinement is further increased to sub-10 nm, the condensate initiates from the nanochannel entrance and grows toward the dead end (Figure 8b), as the gas adsorption at the entrance is much faster than that at the dead end because the vapor transport limit outweighs the influence of the additional end-wall surface. In this case, the condensate growth dynamics is governed simultaneously by both the liquid−vapor interfacial kinetic resistance and the liquid capillary filling dynamics (Figure 8b).[40] The planar nanochannel platform also provided clear identification of a liquid film in front of the capillary filling interface as well as an evaluation of its thickness at a few fluid molecular layers (Figure 8b).

The behavior of nonpolar gas species (e.g., hydrocarbon) condensation at the nanoscale does not fully describe water condensation, where stronger molecule−surface and intermolecular interactions are expected. For example, although the Kelvin equation closely predicts propane condensation at 8 nm, the equation requires modification (even at 10^2 nm confinement) because the adsorbed water layer (up to 200 nm thick) effectively tightens the confinement.[42] Water condensation at the nanoscale occurring earlier than predicted by the Kelvin equation indicates the potential for a lower threshold and a higher efficiency for water harvesting from air or thermal desalination using nanoporous materials.[36]

https://dx.doi.org/10.1021/acs.accounts.9b00411
Acc. Chem. Res. XXXX, XXX, XXX−XXX

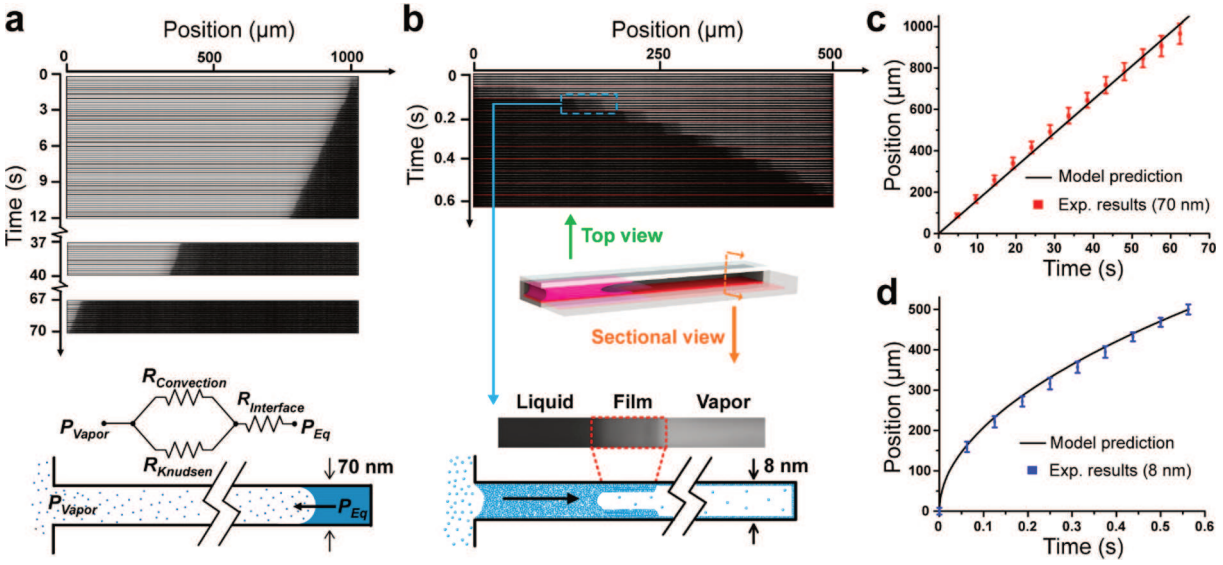

Figure 8. (a, b) Propane condensate growth and model description in (a) a 70 nm-deep channel and (b) an 8 nm-deep channel with different dynamics. (c, d) Comparison of experimental condensate growth with model predictions at (c) 70 nm and (d) 8 nm. Panels a and c are Reproduced from (a, c) ref 41 and (b, d) ref 40. Copyright 2017 and 2018, respectively, American Chemical Society.

5. CONCLUSION AND OUTLOOK

As summarized above, our recent efforts in the direct quantification of nanoscale liquid transport and phase change have resulted in significant new understanding of nanoconfined fluid mechanics and thermodynamics as well as a suite of nanofluidic tools with which to expand on this base. We observed that for polar liquids like water or mixtures in nanoscale-confined spaces, the corresponding fluid properties deviate from the bulk values and their thermodynamic behaviors can no longer be predicted by classical theory because of strong surface−liquid interactions. Our discoveries certainly benefited from the nanochannel planform, which made it possible to directly probe/visualize nanoscale-confined liquids and liquid−vapor interfaces. Much of this work also required new device design, integration, and measurement methods, which enabled us to convert optical images/videos of confined fluids and interfaces into fluid/thermodynamic property measurements.

Looking forward, we expect that nanofluidic devices will continue to play an important role in exploring fundamentals and applications of nanoscale liquid transport and phase change. In particular, we expect these approaches to enable major advances in the following four areas.

5.1. Measuring Thermal Properties

Although nanofluidic technology has greatly informed on nanoscale fluid behaviors, many important fluid/thermophysical properties still remain elusive. Specifically, there is a tremendous need for nanofluidic tools to make thermal measurements, including measurements of thermal conductivity, heat capacity, and latent heat. These properties, together with the observed anomalous fluid behaviors, would enable the development of more efficient cooling systems and novel liquid thermoelectric devices. We expect progress here on two fronts. Microfabricated nanofluidic devices are compatible with on-chip thermal measurement apparatuses, similar to those employed in nanoelectromechanical systems (NEMS) for characterizing the thermal conductivities of 1D and 2D nanomaterials.[43] The key challenge here is to design and fabricate a smart on-chip device to effectively integrate thermal measurement sensors with fluidic nanochannels/nanopores while simultaneously ensuring thermal isolation and minimizing sensor−fluid interactions. The recent developments of on-chip calorimetry[44] and temperature sensing in microfluidic devices[45] provide some inspiration and guidance to address this challenge. At the same time, scanning probe microscopy (SPM) has been applied to detect nanoscale liquid properties from a liquid film confined between the probe and substrate. That method was pioneered to estimate the heat conductivity for a water film at sub-100 nm scale.[46] The combination of SPM and nanofluidic devices with an open but highly controlled window for probing fluids may lead to further breakthroughs in the field.

5.2. Probing Liquid Structures/Compositions

Beyond measurement of thermal properties of nanoscale-confined liquids, another opportunity to explore nanoscale anomalous fluid behaviors is to probe local liquid structures/compositions. Correlating anomalous fluid behaviors with such local information would greatly deepen our understanding of the fundamental mechanisms. For example, direct validation of the immobilized hydration layer near the wall of silica nanochannels and identification of the condensate compositions along the nanochannel height direction would enable us to explain the large deviation between our observations and classical predictions with great confidence.[37] In general, such local structure/composition information can be collected only by using advanced surface/interface-sensitive techniques,[47,48] such as infrared and nonlinear optical spectroscopy, SPM, X-ray-based core-level spectroscopies, and Raman spectroscopy. A major challenge thus involves creating nanochannel devices with ultrathin and "transparent" channel walls to allow these techniques to probe the confined liquids. As thin nanochannels are prone to collapse during liquid introduction because of capillarity-induced negative pressure,[49] both fabrication and handling protocols need to be carefully designed. Another challenge for such local characterization is signal processing and analysis, especially for surface-sensitive spectroscopy techniques, since signals could come from the opposing

https://dx.doi.org/10.1021/acs.accounts.9b00411
Acc. Chem. Res. XXXX, XXX, XXX−XXX

surfaces/interface, which may not share the same chemical composition or structure. If these challenges can be properly addressed, a new level of resolution—and a new level of understanding—would be achieved.

5.3. Exploring Sub-2 nm Nanofluidics

In studying nanofluidic systems with well-defined geometries, we have discovered confinement-dependent fluid behaviors that become more pronounced with increased confinement. However, our discoveries have yet to extend into the sub-2 nm regime, where the nanoscale confinement reaches the extreme case, i.e., only capable of accommodating several liquid molecules in the confined dimension(s). Because in this regime the classical continuity assumption is no longer valid and fluid behaviors were previously only accessible in simulations and nanoporous membranes, accurately measuring fluid behaviors in this regime would guarantee great scientific importance and reveal a rich physics. Additionally, since sub-2 nm conduits are basic constituents of 2D-material-based lamellar and nanotube membranes, insights gained from such studies would also provide guidelines for developing new lamellar and nanotube membranes for various separation and energy applications. There are two major challenges for exploring sub-2 nm nanofluidics using nanofluidic devices. The first one is again a challenge in fabrication. Fabrication of nanoscale confinements at the sub-2 nm scale with semiconductor fabrication processes is still unreliable, since the surface roughness of typical substrates is 0.2−0.5 nm. Fortunately, the emergence of 2D materials (e.g., MoS_2 and graphene) has opened a new avenue to overcome this challenge. Recent studies showed that sub-2 nm nanoslits with well-defined dimensions can be fabricated by van der Waals assembly, enabling several striking discoveries, including ultrafast water capillary flow,[11] size-dependent ion transport,[50] and frictionless gas permeation.[29] The second challenge is that we will need new measurement techniques that can either detect the liquid−vapor interface (which is challenging for optical microscopes because of the ultralow contrast) or directly measure the ultralow flow rates. To date, electrical detection of the interface,[51] ultrasensitive mass balances,[11] and mass spectrometers[50] are the few techniques/apparatuses that have been used for such studies. However, each of them has its own limitations, and new methods that are compatible with 2D-materials-based nanofluidic devices would be a boon.

5.4. Enabling Precise Synthesis/Assembly

As the aforementioned characterization/measurement methods become mature, we envision broad applications of nanofluidics far beyond its traditional applications in biomedicine and separation. In particular, we foresee new applications of nanofluidic devices in enabling precise synthesis/assembly in chemistry and materials science. Microfabricated fluidic devices have already been used as a platform in liquid-phase transmission electron microscopy (LPTEM) to study in situ material synthesis/chemical reactions in confined liquids (100−1000 nm).[52] Importantly, in many cases, nanoscale confinement strongly affects the material synthesis/chemical reactions, e.g., synthesis of 2D nanosheets within nanoreactors[53] and conjugated polymers with controlled conformation in nanotubes.[54] These emerging nanoconfinement-assisted synthesis/assemblies require clear fundamental understanding from controlled experiments. The combination of LPTEM and other methods (e.g., Raman spectroscopy[55]) with purpose-built nanofluidic devices could serve these future experimental needs uniquely well.

In summary, with the advancement of nanofabrication and measurement techniques, it is foreseeable that nanofluidic devices with well-controlled dimensions and surface properties will not only shed light on fundamental nanoscale fluid research but also significantly advance across disciplines such as physics, chemistry, and materials science.

AUTHOR INFORMATION

Corresponding Authors

Chuanhua Duan − *Boston University, Boston, Massachusetts;* orcid.org/0000-0002-5453-5321; Email: duan@bu.edu

David Sinton − *University of Toronto, Toronto, Canada;* orcid.org/0000-0003-2714-6408; Email: sinton@mie.utoronto.ca

Other Authors

Junjie Zhong − *University of Toronto, Toronto, Canada;* orcid.org/0000-0001-6293-9580

Mohammad Amin Alibakhshi − *Boston University, Boston, Massachusetts*

Quan Xie − *Boston University, Boston, Massachusetts;* orcid.org/0000-0002-4670-6899

Jason Riordon − *University of Toronto, Toronto, Canada*

Yi Xu − *University of Toronto, Toronto, Canada;* orcid.org/0000-0002-8108-0975

Complete contact information is available at: https://pubs.acs.org/10.1021/acs.accounts.9b00411

Author Contributions

[⊥]J.Z., M.A.A., and Q.X. contributed equally to this work.

Notes

The authors declare no competing financial interest.

Biographies

Junjie Zhong is a Research Associate at the University of Toronto. His research focuses on micro/nanofluidic device applications in energy and environment.

Mohammad Amin Alibakhshi is currently an associate research scientist at Northeastern University. He got his Ph.D. in Mechanical Engineering from Boston University in 2016. His research focuses on nanofluidics, nanopore sensing, and 2D materials.

Quan Xie is currently a senior coatings engineer at LiquiGlide Inc. He got his Ph.D. in Mechanical Engineering at Boston University in 2018. His research focuses on nanofluidics, 2D materials, and interfacial science.

Jason Riordon is a Research Associate at the University of Toronto. His research focuses on designing lab-on-a-chip systems for a wide range of applications.

Yi Xu is a Ph.D. candidate at the University of Toronto. His research is focused on designing nanoporous systems for CO_2 electroreduction.

Chuanhua Duan is an Assistant Professor at Boston University. His research focuses on the study of micro- and nanofluidic transport phenomena and the development of new fluidic devices/approaches

https://dx.doi.org/10.1021/acs.accounts.9b00411
Acc. Chem. Res. XXXX, XXX, XXX−XXX

for applications in healthcare, thermal management, and energy systems.

David Sinton is a Professor and Canada Research Chair in Microfluidics and Energy at the University of Toronto. His research involves the study and application of small-scale fluid mechanics for use in energy systems and analysis.

■ ACKNOWLEDGMENTS

The Sinton group gratefully acknowledges support from the Natural Sciences and Engineering Research Council of Canada, Canada Research Chairs, and Alberta Innovates. The Duan group thanks the National Science Foundation for support (NSF CBET-1653767 and NSF CBET-1805421).

■ REFERENCES

(1) Sparreboom, W.; van den Berg, A.; Eijkel, J. C. Principles and applications of nanofluidic transport. *Nat. Nanotechnol.* **2009**, *4*, 713.
(2) Wang, C.; Nam, S.-W.; Cotte, J. M.; Jahnes, C. V.; Colgan, E. G.; Bruce, R. L.; Brink, M.; Lofaro, M. F.; Patel, J. V.; Gignac, L. M.; et al. Wafer-scale integration of sacrificial nanofluidic chips for detecting and manipulating single DNA molecules. *Nat. Commun.* **2017**, *8*, 14243.
(3) Siria, A.; Bocquet, M.-L.; Bocquet, L. New avenues for the large-scale harvesting of blue energy. *Nat. Rev. Chem.* **2017**, *1*, No. 0091.
(4) Skaug, M. J.; Schwemmer, C.; Fringes, S.; Rawlings, C. D.; Knoll, A. W. Nanofluidic rocking Brownian motors. *Science* **2018**, *359*, 1505.
(5) Levin, S.; Fritzsche, J.; Nilsson, S.; Runemark, A.; Dhokale, B.; Ström, H.; Sundén, H.; Langhammer, C.; Westerlund, F. A nanofluidic device for parallel single nanoparticle catalysis in solution. *Nat. Commun.* **2019**, *10*, 4426.
(6) Barsotti, E.; Tan, S. P.; Saraji, S.; Piri, M.; Chen, J.-H. A review on capillary condensation in nanoporous media: Implications for hydrocarbon recovery from tight reservoirs. *Fuel* **2016**, *184*, 344.
(7) Lee, J.; Laoui, T.; Karnik, R. Nanofluidic transport governed by the liquid/vapour interface. *Nat. Nanotechnol.* **2014**, *9*, 317.
(8) Li, H.; Zhong, J.; Pang, Y.; Zandavi, S. H.; Persad, A. H.; Xu, Y.; Mostowfi, F.; Sinton, D. Direct visualization of fluid dynamics in sub-10 nm nanochannels. *Nanoscale* **2017**, *9*, 9556.
(9) Rossi, M. P.; Ye, H.; Gogotsi, Y.; Babu, S.; Ndungu, P.; Bradley, J.-C. Environmental scanning electron microscopy study of water in carbon nanopipes. *Nano Lett.* **2004**, *4*, 989.
(10) Secchi, E.; Marbach, S.; Niguès, A.; Stein, D.; Siria, A.; Bocquet, L. Massive radius-dependent flow slippage in carbon nanotubes. *Nature* **2016**, *537*, 210.
(11) Radha, B.; Esfandiar, A.; Wang, F.; Rooney, A.; Gopinadhan, K.; Keerthi, A.; Mishchenko, A.; Janardanan, A.; Blake, P.; Fumagalli, L.; et al. Molecular transport through capillaries made with atomic-scale precision. *Nature* **2016**, *538*, 222.
(12) Vincent, O.; Szenicer, A.; Stroock, A. D. Capillarity-driven flows at the continuum limit. *Soft Matter* **2016**, *12*, 6656.
(13) Rangharajan, K. K.; Mohana Sundaram, P.; Conlisk, A.; Prakash, S. Surface dependent enhancement in water vapor permeation through nanochannels. *Analyst* **2018**, *143*, 4256.
(14) Alibakhshi, M. A.; Xie, Q.; Li, Y.; Duan, C. Accurate measurement of liquid transport through nanoscale conduits. *Sci. Rep.* **2016**, *6*, 24936.
(15) Xie, Q.; Alibakhshi, M. A.; Jiao, S.; Xu, Z.; Hempel, M.; Kong, J.; Park, H. G.; Duan, C. Fast water transport in graphene nanofluidic channels. *Nat. Nanotechnol.* **2018**, *13*, 238.
(16) Wu, K.; Chen, Z.; Li, J.; Li, X.; Xu, J.; Dong, X. Wettability effect on nanoconfined water flow. *Proc. Natl. Acad. Sci. U. S. A.* **2017**, *114*, 3358.
(17) Zhang, X.; Liu, H.; Jiang, L. Wettability and applications of nanochannels. *Adv. Mater.* **2019**, *31*, 1804508.
(18) Park, H. G.; Jung, Y. Carbon nanofluidics of rapid water transport for energy applications. *Chem. Soc. Rev.* **2014**, *43*, 565.
(19) Xue, G.; Xu, Y.; Ding, T.; Li, J.; Yin, J.; Fei, W.; Cao, Y.; Yu, J.; Yuan, L.; Gong, L.; Chen, J.; Deng, S.; Zhou, J.; Guo, W. Water-evaporation-induced electricity with nanostructured carbon materials. *Nat. Nanotechnol.* **2017**, *12*, 317.
(20) Ghasemi, H.; Ni, G.; Marconnet, A. M.; Loomis, J.; Yerci, S.; Miljkovic, N.; Chen, G. Solar steam generation by heat localization. *Nat. Commun.* **2014**, *5*, 4449.
(21) Persad, A. H.; Ward, C. A. Expressions for the evaporation and condensation coefficients in the Hertz−Knudsen relation. *Chem. Rev.* **2016**, *116*, 7727.
(22) Li, Y.; Alibakhshi, M. A.; Zhao, Y.; Duan, C. Exploring Ultimate Water Capillary Evaporation in Nanoscale Conduits. *Nano Lett.* **2017**, *17*, 4813.
(23) Li, Y.; Chen, H.; Xiao, S.; Alibakhshi, M. A.; Lo, C.-W.; Lu, M.-C.; Duan, C. Ultrafast Diameter-Dependent Water Evaporation from Nanopores. *ACS Nano* **2019**, *13*, 3363.
(24) Lu, Z.; Kinefuchi, I.; Wilke, K. L.; Vaartstra, G.; Wang, E. N. A unified relationship for evaporation kinetics at low Mach numbers. *Nat. Commun.* **2019**, *10*, 2368.
(25) Xie, Q.; Xiao, S.; Duan, C. Geometry-Dependent Drying in Dead-End Nanochannels. *Langmuir* **2017**, *33*, 8395.
(26) Eijkel, J. C.; Dan, B.; Reemeijer, H.; Hermes, D.; Bomer, J. G.; van den Berg, A. Strongly accelerated and humidity-independent drying of nanochannels induced by sharp corners. *Phys. Rev. Lett.* **2005**, *95*, 256107.
(27) Jatukaran, A.; Zhong, J.; Persad, A. H.; Xu, Y.; Mostowfi, F.; Sinton, D. Direct Visualization of Evaporation in a Two-Dimensional Nanoporous Model for Unconventional Natural Gas. *ACS Appl. Nano Mater.* **2018**, *1*, 1332.
(28) Jatukaran, A.; Zhong, J.; Abedini, A.; Sherbatian, A.; Zhao, Y.; Jin, Z.; Mostowfi, F.; Sinton, D. Natural gas vaporization in a nanoscale throat connected model of shale: multi-scale, multi-component and multi-phase. *Lab Chip* **2019**, *19*, 272.
(29) Keerthi, A.; Geim, A.; Janardanan, A.; Rooney, A.; Esfandiar, A.; Hu, S.; Dar, S.; Grigorieva, I.; Haigh, S.; Wang, F.; Radha, B. Ballistic molecular transport through two-dimensional channels. *Nature* **2018**, *558*, 420.
(30) Jun, Y.-S.; Zhang, L.; Min, Y.; Li, Q. Nanoscale chemical processes affecting storage capacities and seals during geologic CO_2 sequestration. *Acc. Chem. Res.* **2017**, *50*, 1521.
(31) Duan, C.; Karnik, R.; Lu, M.-C.; Majumdar, A. Evaporation-induced cavitation in nanofluidic channels. *Proc. Natl. Acad. Sci. U. S. A.* **2012**, *109*, 3688.
(32) Bao, B.; Zandavi, S. H.; Li, H.; Zhong, J.; Jatukaran, A.; Mostowfi, F.; Sinton, D. Bubble nucleation and growth in nano-channels. *Phys. Chem. Chem. Phys.* **2017**, *19*, 8223.
(33) Nosonovsky, M.; Bhushan, B. Phase behavior of capillary bridges: towards nanoscale water phase diagram. *Phys. Chem. Chem. Phys.* **2008**, *10*, 2137.
(34) Vincent, O.; Sessoms, D. A.; Huber, E. J.; Guioth, J.; Stroock, A. D. Drying by cavitation and poroelastic relaxations in porous media with macroscopic pores connected by nanoscale throats. *Phys. Rev. Lett.* **2014**, *113*, 134501.
(35) Cho, H. J.; Preston, D. J.; Zhu, Y.; Wang, E. N. Nanoengineered materials for liquid−vapour phase-change heat transfer. *Nat. Rev. Mater.* **2017**, *2*, 16092.
(36) Kim, H.; Yang, S.; Rao, S. R.; Narayanan, S.; Kapustin, E. A.; Furukawa, H.; Umans, A. S.; Yaghi, O. M.; Wang, E. N. Water harvesting from air with metal−organic frameworks powered by natural sunlight. *Science* **2017**, *356*, 430.
(37) Zhong, J.; Zhao, Y.; Lu, C.; Xu, Y.; Jin, Z.; Mostowfi, F.; Sinton, D. Nanoscale Phase Measurement for the Shale Challenge: Multi-component Fluids in Multiscale Volumes. *Langmuir* **2018**, *34*, 9927.
(38) Abdel Hamid, A. R.; Mhanna, R.; Lefort, R.; Ghoufi, A.; Alba-Simionesco, C.; Frick, B.; Morineau, D. Microphase separation of binary liquids confined in cylindrical pores. *J. Phys. Chem. C* **2016**, *120*, 9245.
(39) Zhuang, T.-T.; Pang, Y.; Liang, Z.-Q.; Wang, Z.; Li, Y.; Tan, C.-S.; Li, J.; Dinh, C. T.; De Luna, P.; Hsieh, P.-L.; Burdyny, T.; Li, H.-

https://dx.doi.org/10.1021/acs.accounts.9b00411
Acc. Chem. Res. XXXX, XXX, XXX−XXX

H.; Liu, M.; Wang, Y.; Li, F.; Proppe, A.; Johnston, A.; Nam, D.-H.; Wu, Z.-Y.; Zheng, Y.-R.; Ip, A. H.; Tan, H.; Chen, L.-J.; Yu, S.-H.; Kelley, S. O.; Sinton, D.; Sargent, E. H. Copper nanocavities confine intermediates for efficient electrosynthesis of C3 alcohol fuels from carbon monoxide. *Nat. Catal.* **2018**, *1*, 946.

(40) Zhong, J.; Riordon, J.; Zandavi, S. H.; Xu, Y.; Persad, A. H.; Mostowfi, F.; Sinton, D. Capillary Condensation in 8 nm Deep Channels. *J. Phys. Chem. Lett.* **2018**, *9*, 497.

(41) Zhong, J.; Zandavi, S. H.; Li, H.; Bao, B.; Persad, A. H.; Mostowfi, F.; Sinton, D. Condensation in One-Dimensional Dead-End Nanochannels. *ACS Nano* **2017**, *11*, 304.

(42) Fisher, L.; Gamble, R.; Middlehurst, J. The Kelvin equation and the capillary condensation of water. *Nature* **1981**, *290*, 575.

(43) Estrada, D.; Li, Z.; Choi, G.-M.; Dunham, S. N.; Serov, A.; Lee, J.; Meng, Y.; Lian, F.; Wang, N. C.; Perez, A.; et al. Thermal transport in layer-by-layer assembled polycrystalline graphene films. *npj 2D Mater. Appl.* **2019**, *3*, 10.

(44) Krenger, R.; Lehnert, T.; Gijs, M. A. Dynamic microfluidic nanocalorimetry system for measuring *Caenorhabditis elegans* metabolic heat. *Lab Chip* **2018**, *18*, 1641.

(45) Yang, F.; Yang, N.; Huo, X.; Xu, S. Thermal sensing in fluid at the micro-nano-scales. *Biomicrofluidics* **2018**, *12*, No. 041501.

(46) Assy, A.; Lefèvre, S.; Chapuis, P.-O.; Gomès, S. Analysis of heat transfer in the water meniscus at the tip−sample contact in scanning thermal microscopy. *J. Phys. D: Appl. Phys.* **2014**, *47*, 442001.

(47) Björneholm, O.; Hansen, M. H.; Hodgson, A.; Liu, L.-M.; Limmer, D. T.; Michaelides, A.; Pedevilla, P.; Rossmeisl, J.; Shen, H.; Tocci, G.; et al. Water at interfaces. *Chem. Rev.* **2016**, *116*, 7698.

(48) Agrawal, K. V.; Shimizu, S.; Drahushuk, L. W.; Kilcoyne, D.; Strano, M. S. Observation of extreme phase transition temperatures of water confined inside isolated carbon nanotubes. *Nat. Nanotechnol.* **2017**, *12*, 267.

(49) Tas, N. R.; Mela, P.; Kramer, T.; Berenschot, J. W.; van den Berg, A. Capillarity induced negative pressure of water plugs in nanochannels. *Nano Lett.* **2003**, *3*, 1537.

(50) Esfandiar, A.; Radha, B.; Wang, F.; Yang, Q.; Hu, S.; Garaj, S.; Nair, R.; Geim, A.; Gopinadhan, K. Size effect in ion transport through angstrom-scale slits. *Science* **2017**, *358*, 511.

(51) Qin, X.; Yuan, Q.; Zhao, Y.; Xie, S.; Liu, Z. Measurement of the rate of water translocation through carbon nanotubes. *Nano Lett.* **2011**, *11*, 2173.

(52) Ross, F. M. Opportunities and challenges in liquid cell electron microscopy. *Science* **2015**, *350*, aaa9886.

(53) Li, Z.; Zhang, X.; Cheng, H.; Liu, J.; Shao, M.; Wei, M.; Evans, D. G.; Zhang, H.; Duan, X. Confined Synthesis of 2D Nanostructured Materials toward Electrocatalysis. *Adv. Energy Mater.* **2019**, 1900486.

(54) Duvail, J.; Retho, P.; Fernandez, V.; Louarn, G.; Molinie, P.; Chauvet, O. Effects of the confined synthesis on conjugated polymer transport properties. *J. Phys. Chem. B* **2004**, *108*, 18552.

(55) Sugano, K.; Suekuni, K.; Takeshita, T.; Aiba, K.; Isono, Y. Surface-enhanced Raman spectroscopy using linearly arranged gold nanoparticles embedded in nanochannels. *Jpn. J. Appl. Phys.* **2015**, *54*, No. 06FL03.

https://dx.doi.org/10.1021/acs.accounts.9b00411
Acc. Chem. Res. XXXX, XXX, XXX−XXX